International Journal of Heat and Technology
Vol. 40, No. 1, February, 2022, pp. 1-8
Journal homepage: http://iieta.org/journals/ijht

Experimental Study of a Direct Immersion Liquid Cooling of a Li-Ion Battery for Electric Vehicles Applications

Luca Giammichele*, Valerio D'Alessandro, Matteo Falone, Renato Ricci

Dipartimento di Ingegneria Industriale e Scienze Matematiche, Università Politecnica delle Marche, Via Brecce Bianche 12, 60131 Ancona (AN), Italy

Corresponding Author Email: l.giammichele@staff.univpm.it

https://doi.org/10.18280/ijht.400101

Received: 25 January 2022
Accepted: 15 February 2022

Keywords:
dielectric fluid, direct contact liquid cooling, lithium-ion batteries, thermal management system

ABSTRACT

The aim of this work is to test a battery thermal management system by direct immersion of a commercial 18650 $LiFePO_4$ cell in a low boiling dielectric liquid. It is worth noting that for electric mobility applications, thermal management of Lithium-Ion batteries is a fundamental issue because batteries experience high discharge currents and temperatures. First, we present an electrical characterization of the Lithium-Ion by measuring cell potential, open circuit potential and entropic heat coefficient. Temperature measurements were carried out with thermocouples and infrared thermography. A simplified heat generation term was evaluated using the experimental data. Then, the same battery was immersed in a dielectric low boiling liquid and tested under three different discharge currents. For comparison, also the case without dielectric liquid was analyzed. This paper demonstrates the feasibility of a thermal management system based on direct immersion of a battery cell in a low boiling dielectric fluid. Indeed, the results show a substantial decrease of battery temperature when immersed.

1. INTRODUCTION

Nowadays sustainable mobility is a fundamental issue for emission reduction and energy saving. Minimize environmental impact is a primary objective in our daily life and electric vehicles (EVs) development and commercialization play a central role in this context [1, 2].

Lithium-Ion batteries (Li-Ion) are the most commonly adopted power supply for EVs. They have the following advantages: lighter weight, higher energy density and specific power, longer cycle life, lower self-discharge rates and higher recyclability [3-5].

Although from an electrochemical point of view this technology was optimized, Li-Ion batteries thermal management is still an open challenge. Indeed, the extreme operating temperatures, charge/discharge currents and the state of charge (SOC) accelerate the ageing process. In particular, temperature has a remarkable effect on the performance degradation and lifetime of Li-Ion cells [6, 7].

This is a fundamental issue since several literature studies are dedicated to the Battery Thermal Management System (BTMS). More in depth, in the open literature, different cooling strategies are used for this purpose. The simplest methods are air cooling systems, in forced or natural convection. In these cases, also a heat sinks/pin-fins are usually adopted to enhance the heat transfer [8, 9]. However, for EVs applications, liquid cooling methods are more effective because of their high thermal capacity. This technology was applied with a single-phase or two-phase refrigerant [10, 11], or using nano-fluids [12] that flows into a heat exchanger rounding the power module's cells. In this configuration a further thermal resistance is introduced by the heat exchanger. Moreover, in the last years it was analyzed the performance of innovative BTMS such as Phase Change Materials (PCM) [13, 14], Heat Pipes (HP) [15, 16], and Pulsating Heat Pipes (PHP) [17].

Recently, also a direct contact liquid cooling has been presented. In order to avoid short circuit on the battery terminal, a dielectric fluid must be considered as coolant. This system has several advantages: the thermal power generated is directly transferred to the coolant without any other element, larger heat transfer surface area, higher uniformity in the temperature distribution, and the cooling system is simpler and lightweight [18]. Only some papers are devoted to direct immersion liquid cooling strategies [19-22]. Patil et al. [19], investigate the effect of different cooling strategies on a large-format pouch cell both experimentally and numerically. They used a dielectric fluid in static and flowing conditions, considering also tab cooling. Wu et al. [20], design a lithium-ion battery thermal management system based direct immersion in a silicone oil. The results show that the maximum temperature rise of the direct contact liquid cooling system is only 20% of the indirect contact liquid cooling system. Wu et al. [21], used a low boiling dielectric liquid as a coolant for a pouch cell. The experimental results show an excellent capability of the system in reducing maximum temperature and improving temperature uniformity. Wang and Wu [22], studied the cooling effect of a low boiling dielectric fluid in forced convection for a cylindrical battery pack.

In this context, is a crucial issue to evaluate the battery thermal power generation. A correct determination of this parameter for a single cell allows to improve the BTMS design method. The battery heat generation is related to different mechanisms: activation of interfacial kinetics, concentration species transport, and ohmic Joule heating from the movement of charged particles, which becomes very significant for large

cell sizes [23]. Two main contributions to the heat generation are usually adopted in literature: the irreversible heat and the reversible heat generation. The first term is due to the Joule losses over cell internal resistance, mass transfer limitations in the cell components, and charge transfer overpotentials at the interface. The second term depends on the entropic heat coefficient (EHC) which is related to the nature of electrochemical reaction in the cell and battery composition. The entropic contribution has a substantial influence on heat generation and cannot be neglected or considered constant with SOC. Indeed, it could assume a value similar to the irreversible term especially for low discharge currents [24-27]. Rad et al. [28], show that also battery surface temperature is affected by the entropic heat. In literature the EHC is usually measured through potentiometric test [24, 25, 29, 30]. Thomas et al. [29], state that is more useful to modify the temperature at a specific SOC. Nieto et al. [24], state that charge or discharge processes do not influence the entropic heat coefficient. The temperatures chosen for the thermal cycle have a little influence on EHC. This was also confirmed by Madani et al. [30].

This paper presents an experimental investigation of a novel cooling strategy for Li-Ion batteries based on a low boiling dielectric liquid. The battery is directly submerged in the cooling fluid. The low boiling characteristic is a fundamental issue since the change of phase ensures the absorption of heat power peaks due to the instantaneous electric power required from the electric motor. First, an electrical and thermal characterization of the Lithium-Ion battery was performed under three different operating currents. The open circuit potential and entropic heat coefficient were experimentally measured. These data were used to calculate the battery heat generation with a simplified equation. Then the thermal behavior of the cell submerged in the dielectric liquid was investigated under several operating currents. Both constant and impulsive current conditions were tested. For comparison, the same tests were performed without the liquid.

The paper is organised as follows. Section 2 describes the equation used for the calculation of the heat generated. Section 3 presents the experimental setup. Section 4 shows the results of the cell characterization. Section 5 is devoted to the evaluation of battery heat generation. Section 6 presents the results of the novel cooling strategy. Finally, the conclusions are presented in Section 7.

2. HEAT GENERATION MODEL

A complete thermodynamic energy balance for Li-ion batteries was proposed by Bernardi et al. [31]. Eq. (1) is commonly adopted in present studies to evaluate heat generation in Li-ion battery [23-25, 29]:

$$\dot{Q} = \dot{Q}_{irr} + \dot{Q}_{rev} = I \cdot (V - U_{OC}) + I \cdot T \cdot \frac{\partial U_{OC}}{\partial T} \qquad (1)$$

where, I is the discharge current, V is the cell potential, T is the battery surface temperature (expressed in K), $\partial U_{OC}/\partial T$ is the EHC, and U_{OC} is the open circuit potential.

The cell overpotential influences the irreversible term of Eq. (1); it is equal to the difference between V and U_{OC}. This term account for all irreversible processes such as the energy dissipated in electrode overpotentials and Joule heating within the battery internal resistance. In this study, the operating current was considered negative during discharge. For this reason, the irreversible term is always positive.

The electrochemical reaction influenced the reversible term in Eq. (1), which is strongly connected to the EHC. This coefficient can be negative or positive; the reversible heat is exothermic if EHC has a negative value, whereas a positive value of EHC indicates that reversible heat is endothermic during the discharge.

The instantaneous energy dispersed in the form of heat generation can be also determined:

$$E_d = \dot{Q} \cdot \Delta t \qquad (2)$$

where, Δt is the time interval at which the heat was generated. Eq. (3) allows to evaluate the total amount of dispersed energy, given by the sum of instantaneous dispersed energy during the time τ required to fully discharge the battery at the operating current.

$$E_{acc} = \int_0^\tau E_d \, dt \qquad (3)$$

3. EXPERIMENTAL APPARATUS

The battery cell used in this study is a commercial $LiFePO_4$ battery (ENERpower 18650). It is a cylindrical cell of height 65 mm, diameter 18 mm, and weight 42 g. The nominal cell potential was 3.2 V and the maximum voltage when fully charged was 3.65 V. The cell nominal capacity was 1.8 Ah, while the maximum continuous discharge current is 5.4 A.

A programmable power supply (RMX-4125) and DC electronic load (RMX-4005) allow to control the battery charge and discharge processes. The electronic load has a current setting accuracy equal to ±0.1% F.S. in the range 0-70 A and a resolution of 2 mA. A current transducer was used to measure the operating current. The instrument uncertainty is ±0.02 A in the range ±85 A. Ambient temperature and relative humidity were measured with an uncertainty of ±0.6°C and ±2.5%, respectively. Transducer signals of the current and ambient parameters and the cell potential were acquired using the NI 6289 data acquisition device. The resolution of the device is of 0.076 mV in the range 0-10 V with an uncertainty of ±0.25 mV (Figure 1).

The cell surface temperature was measured by four T-type thermocouples placed along the height of the battery with a high-conductivity adhesive. The thermocouples were attached to an ice point reference before being acquired by the data logger. A calibration of the thermocouples, into a high-precision bath, allows to obtain an uncertainty of ±0.05°C. Infrared thermography analysis was performed to qualitatively evaluate the surface temperature distribution using a FLIR SC3000 IR camera. The instrument was equipped with a 320 x 240 QWIP sensor array and a 20° lens with a 20° x 15° field of view with a minimum focus distance of 0.3 m. The thermal sensitivity was 20 mK at 30°C, with an uncertainty of ±1% of the measured value. The battery was covered with black matte paint with an emissivity of 0.94.

During discharge, cell potential, operating current, and surface temperature were continuously acquired at 10 Hz, while IR images were recorded at 1 Hz. Each image was subtracted from the first thermal image taken as reference for the initial condition. The battery temperature used in Eq. (1) is the mean value of the four thermocouples.

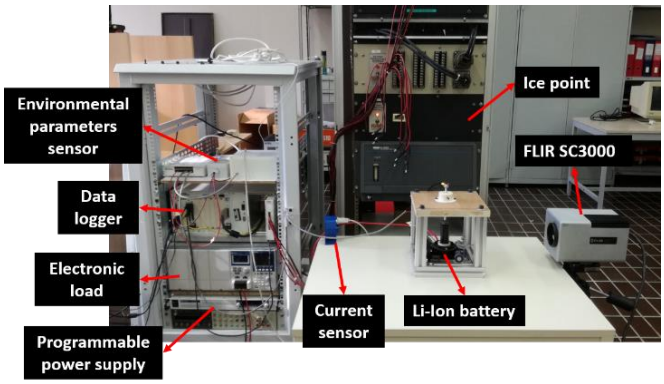

Figure 1. Experimental setup

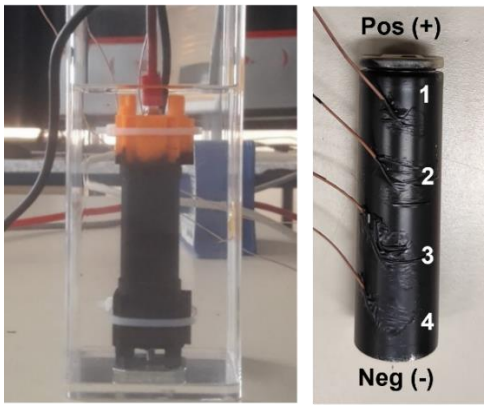

Figure 2. Setup of experimental tests with Novec 7000 (left) and thermocouples arrangement on the battery surface (right)

A different setup was adopted for the liquid cooling tests (Figure 2). The experimental apparatus was the same but, this time, the battery was placed in a plexiglass container of dimensions 50 x 50 x 150 mm. The cell was positioned vertically and in the center of the container which was filled with the dielectric liquid so that the battery was completely submerged. A high-resolution camera was placed in front of the cell to observe the boiling behavior of the cooling liquid. Another T-type thermocouple was placed in the liquid near the wall at 10 mm from the battery surface in order to observe the fluid temperature during the tests.

The dielectric liquid used for the experiments is the Novec 7000 which has a dielectric constant equal to 7.4 and a dielectric strength of 40 kV. It was chosen because of the dielectric properties and for its low boiling point (34°C). Its main physical properties are reported in Table 1.

Table 1. Physical properties of the Novec 7000

λ [W/mK]	C_p [J/kg K]	ρ [kg/m^3]	α [m^2/s]	Pr
0.075	1300	1400	$4.12 \cdot 10^{-8}$	4.85

Table 2. Measurement uncertainties

C-rate	Q_{irr} %	Q_{rev} %	Q %	E_{acc} %
0.5	1.14	0.77	5.52	2.68
1	0.53	0.58	1.06	1.08
2	0.26	0.52	0.35	0.54
3	0.18	0.49	0.23	0.35

The measurement uncertainties were evaluated for all the entities involved. The uncertainty of U_{OC} is ±0.25 mV, while for the EHC is ±0.001 mV/K. The uncertainty of the SOC calculation is related to the setting current accuracy of the electronic load and the measurement uncertainty of the current transducer; we obtained a value of ±0.5%. Table 2 reports the measurement uncertainties of the correlated quantities. For compactness, the largest percentage uncertainty for each C-rate is reported. The C-rate is defined as the ratio between the discharge current applied and the discharge current under which the battery delivers its nominal capacity per hour.

4. CELL CHARACTERIZATION

The evaluation of the Li-Ion battery heat generation requires the determination of different parameters. It is necessary to measure the open circuit potential and the EHC. These quantities were evaluated every 10% of the SOC starting from a battery fully charged until the complete discharge. EHC was measured through the potentiometric method, and U_{OC} with subsequent cycles of discharge and relaxation.

4.1 Open circuit potential

The battery was discharged to a specific SOC at 1C discharge rate. This phase was followed by a relaxation of 1 h. The cell potential reached at the end of relaxation corresponded to the U_{OC}. The U_{OC} used in Eq. (1) is the mean value obtained by 5 different measurements of the open circuit potential; it is also shown in the plots in Figure 3. The maximum percentage deviation of the tests from the mean value was 0.07%.

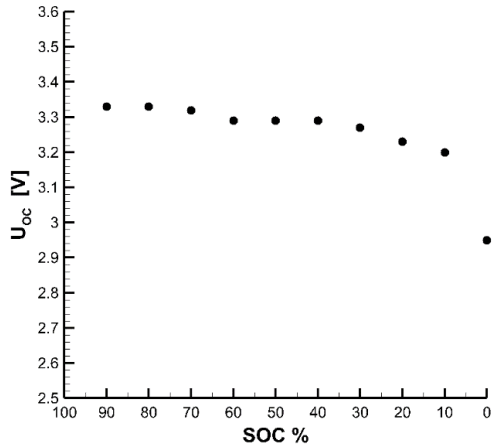

Figure 3. Open circuit potential

4.2 Entropic heat coefficient

The battery was discharged to a specific SOC and was allowed to relax. The relaxation was followed by a thermal cycle in a thermostatic bath. Meanwhile, the open circuit potential of the battery was constantly measured. The thermal cycle used consisted of 3 h at 25°C, 3 h at 10°C, 3 h at 35°C, 3 h at 45°C, and 3 h at 25°C.

This procedure was repeated every 10% of SOC until the battery was completely discharged. Figure 4 shows the open circuit potential variation during the thermal cycle for SOC 50%. The mean voltage value of the last 15 min of each temperature step identifies the U_{OC}. These values were plotted as a function of temperature, as shown in Figure 5. The EHC

corresponds to the gradient of the curve. Finally, the EHC values obtained are reported in Figure 6 as a function of SOC. The EHC has a positive value until 30% of SOC; subsequently, it assumes negative values.

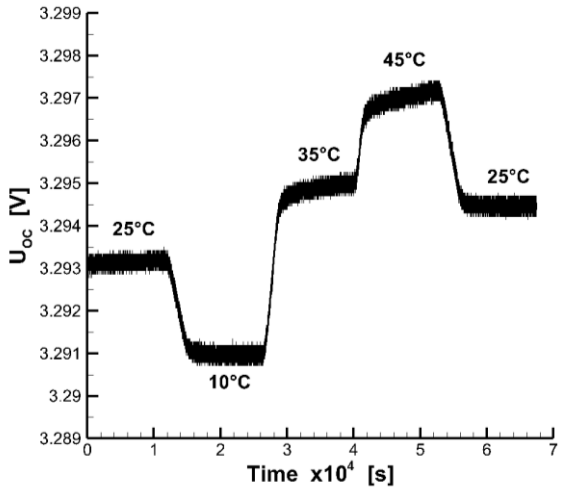

Figure 4. Open circuit potential variation during thermal cycle at SOC 50%

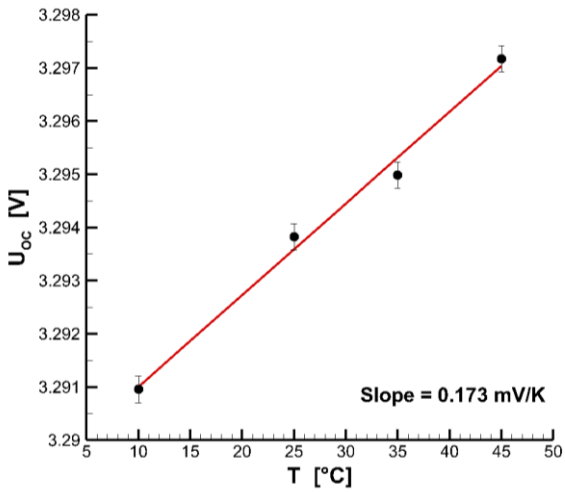

Figure 5. U_{OC} as a function of temperature at SOC 50%

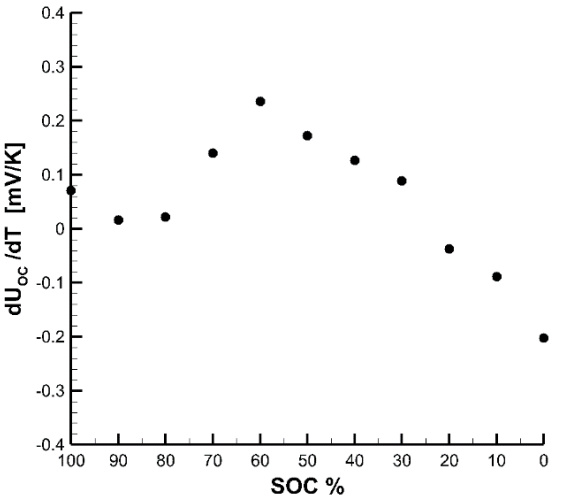

Figure 6. Entropic heat coefficient as a function of SOC

5. DETERMINATION OF THE HEAT GENERATED

The thermal power generated can be evaluated using Eq. (1) for a constant current discharge.

The battery was fully discharged with a constant operating current until the minimum voltage of 2.5 V. The charge method used is the constant current constant voltage procedure: first, a constant current of 1C was applied until the maximum voltage of 3.65 V (CC phase); then, the voltage stays constant and the operating current decreases until a value of 18 mA (CV phase). The test was performed at ambient temperature and under several C-rates (Table 3).

Table 3. Constant current discharge tests

C-rate	Current [A]	Time [s]
1	1.8	3600
2	3.6	1800
3	5.4	1200

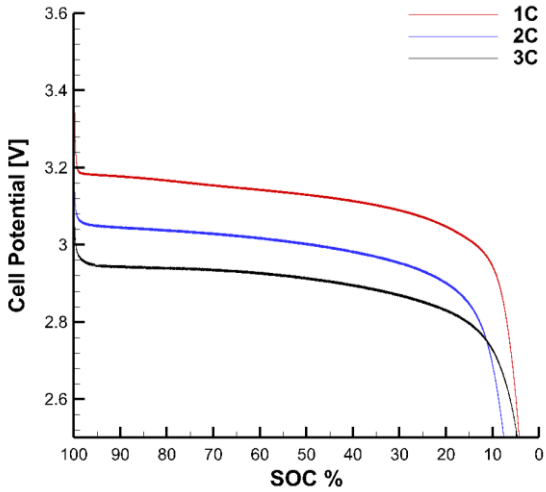

Figure 7. Cell potential for different C-rates

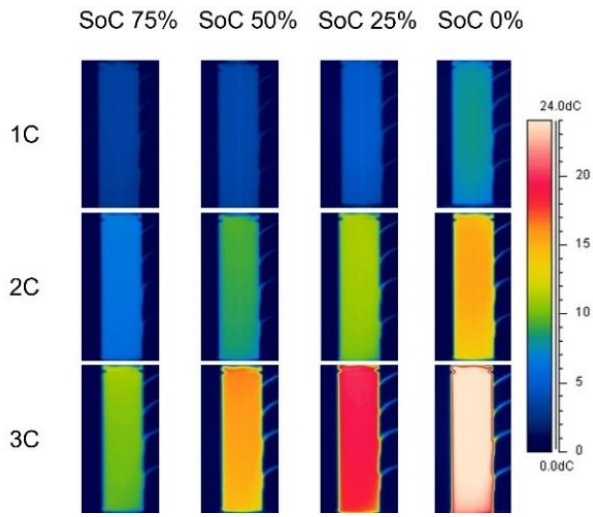

Figure 8. Thermal images of the battery

Figure 7 shows the cell potential as a function of the SOC at different discharge rates. The battery internal resistance produces a sudden fall of the cell potential, then it flattens until a very low SOC. For a higher discharge current, the voltage value of the flattened zone decreases, and the difference with

the open circuit potential increases. Meanwhile, the surface temperature of the battery increases, especially at low SOC.

Figure 8 shows the thermal images acquired during the tests subtracted to a reference image recorded before the discharge starts. Four SOC levels were chosen as representative points for the discharge: 75%, 50%, 25%, and 0%. From infrared images, a higher current produces a higher temperature rise. Indeed, the battery surface temperature reaches very high value for 3C case, far exceeding its operating temperature range. This trend is also confirmed by thermocouples measurements.

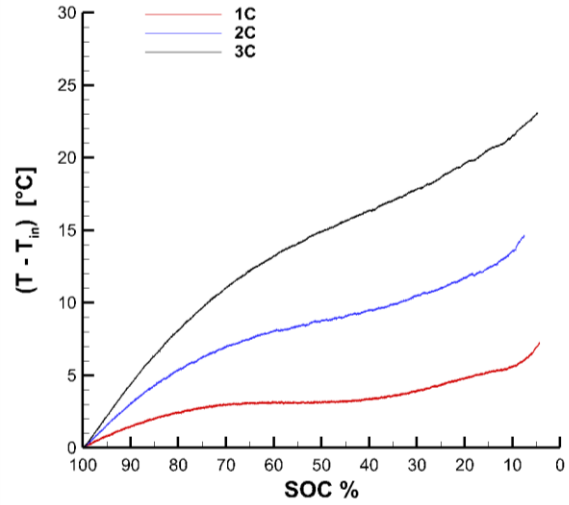

Figure 9. Battery surface temperature measured using thermocouples

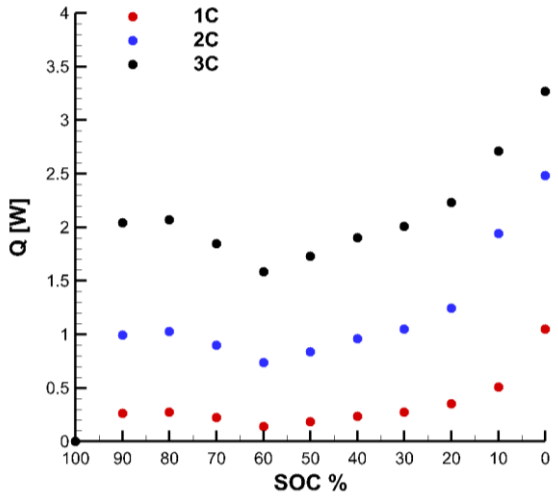

Figure 10. Thermal power generated

Figure 9 shows the mean temperature of the four thermocouples. It can be notice that the greater increase of temperature corresponds to low SOC, when the voltage sharply decreases.

The surface temperature measured by thermocouples was used in Eq. (1) in order to evaluate the total thermal power generated. Figures 10 and 11 show the instantaneous thermal power and the accumulated heat through the discharge process for all C-rates tested. The increase of C-rate leads to higher thermal power and accumulated heat because the overpotential increases with the discharge current. The increase of thermal power is even more marked at low SOC, where the EHC assumes negative values and the cell potential has an abrupt decay. Indeed, the reversible term of Eq. (1) assumes positive values, the discharge process is exothermic, and it increases the total thermal power generated. Otherwise, the reversible term is negative when the EHC is positive, and the discharge process is endothermic. In this situation this term is subtracted from the total heat generation. Both thermal power and accumulated heat are strongly influenced by the reversible term of Eq. (1).

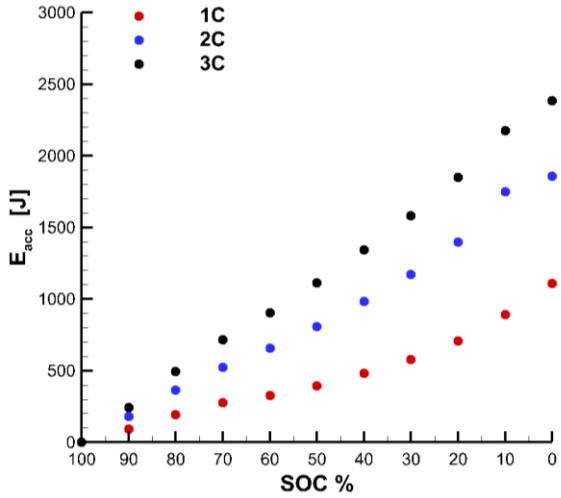

Figure 11. Accumulated energy

6. LIQUID COOLING RESULTS

The cell was submerged in the dielectric liquid (Figure 2) and the same discharge currents were applied. For comparison, also the case without liquid was investigated. The tests were repeated at two different ambient temperatures, 26°C and 32°C.

Figure 12 shows the mean temperature of the battery measured by thermocouples. The results of the three C-rates at the two different ambient temperatures are presented. The solid green line represents the boiling point of the Novec 7000 (34°C). The figure points out the different behavior of the battery surface temperature related to the change of phase of the dielectric liquid. Indeed, for the tests at 26°C the temperature is far from the liquid boiling point and the trend is quite similar to the case without liquid (Figure 9). Furthermore, also the 1C discharge curve at 32°C has the same behavior of the same discharge rate at 26°C because the temperature is always under the boiling point. The temperature plot substantially changes for the 2C and 3C discharges at 32°C. In these cases, the temperature overcomes the boiling point already at 90% of SOC. After that point, the temperature value is almost constant due to the greater amount of heat absorbed by the change of phase of the liquid.

The effectiveness of the liquid cooling is even more evident in Figure 13. The plot shows the temperature difference between the battery surface temperature during discharge and its initial value for three cases: without liquid (black line), with Novec 7000 at 26°C, and with Novec 7000 at 32°C. For compactness, only the 3C test is showed. The temperature difference at the end of discharge without liquid is very large if compared with the liquid cooling cases, and it further decreases when the temperature overcomes the liquid boiling point. Table 4 reports the temperature difference at the end of discharge for all the tests performed.

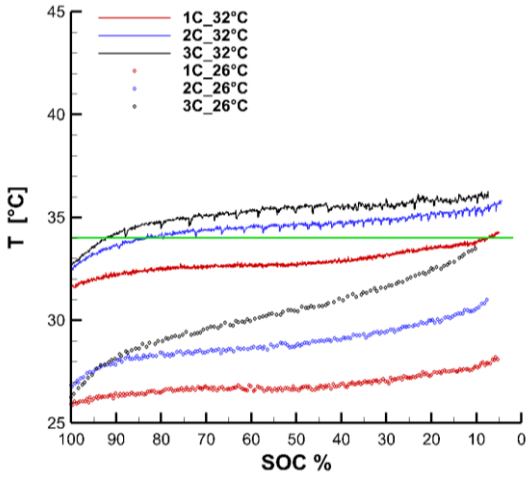

Figure 12. Surface temperature of the submerged battery for different C-rates and ambient temperatures

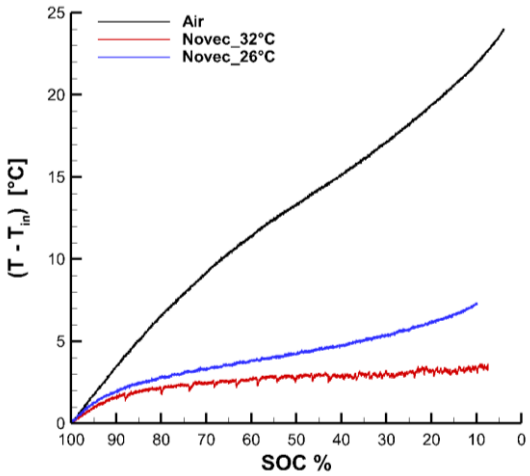

Figure 13. Battery surface temperature for the 3C discharge

Table 4. Temperature difference at the end of discharge

C-rate	Air [°C]	Novec_26°C [°C]	Novec_32°C [°C]
1	5.6	2.3	2.6
2	15.1	4.2	3.3
3	24	7.2	3.6

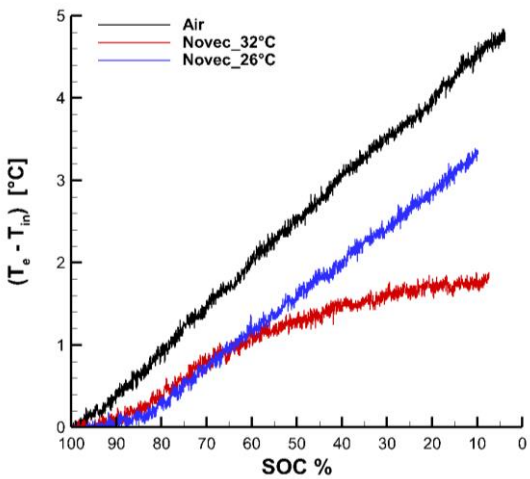

Figure 14. Temperature inside the container for the 3C discharge

Figure 14 shows the temperature difference between the value measured by the thermocouple placed near the wall of the container and its initial value for a 3C discharge. The temperature of the liquid in the measure point is always under the temperature measured without liquid. This is due to the very low thermal diffusivity of the Novec 7000 (Table 1) compared to the air ($1.9 \cdot 10^{-5}$ m^2/s). Indeed, the heat generated by the battery spreads slower in the liquid and the temperature in the measure point is lower at the same SOC. Furthermore, the increase of temperature is linear for the test at 26°C where the liquid temperature is far from the boiling point. The test at 32°C has the same behavior until the 65% of SOC. After that point, the temperature increases with lower intensity due to the change of phase of the liquid. Indeed, the zone of the liquid interested by the change of phase, located near the battery, absorbs a greater amount of thermal power, and the heat spreads even slower in the measure zone.

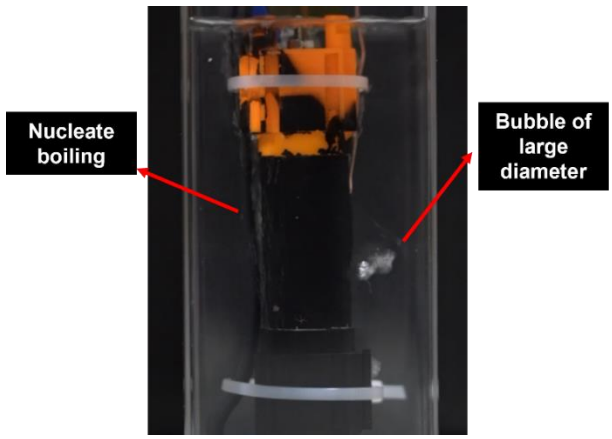

Figure 15. Bubbles formation on battery surface

In Figure 12 and 13 it is interesting to notice that the temperature presents some instantaneous decreases for the 2C and 3C discharges that appears more and more frequently as the SOC decreases. This phenomenon can be related to the boiling formation during the discharges. Figure 15 shows the image of the battery during the 3C discharge, where a nucleate boiling can be detected on the battery surface. Moreover, there is a formation of two types of bubbles. On the battery lateral surface there is the formation of little diameter bubbles that moving continuously upward. Some other bubbles of greater diameter are generated below the battery negative electrode, where they stay until they move upward with a certain frequency.

Finally, an impulsive discharge current was applied to the battery. The discharging cycle used in this test consisted of 25 s at 3C (5.4 A) and 5 s at 10C (18 A). The cycle was stopped when the battery reaches the 30% of SOC in order to avoid damaging the cell. The ambient temperature during the tests was 26°C. Figure 16 shows the temperature measured with and without coolant. It is immediately clear that the dielectric liquid has a great effect on the battery surface temperature, which increases its value of only 8°C. Otherwise, without coolant, the temperature at the end of discharge is 38°C greater than its initial value. In both cases, the temperature has a change of slope when the 10C impulse occurs because the battery generates instantaneously a higher thermal power, and the temperature increases faster. The temperature increases with lower intensity when the current returns to 5.4 A. However, it can be noticed that the temperature decreases its

value, when the current applied is equal to 5.4 A, from the 60% and 90% of SOC respectively in the case without coolant and with the dielectric liquid. This behavior can be explained since the increase of surface temperature creates a convective motion of higher intensity that leads to a higher heat transfer. The lower discharge current (3C) generates a lower thermal power that is completely dissipated by the convective heat transfer, and the temperature decreases.

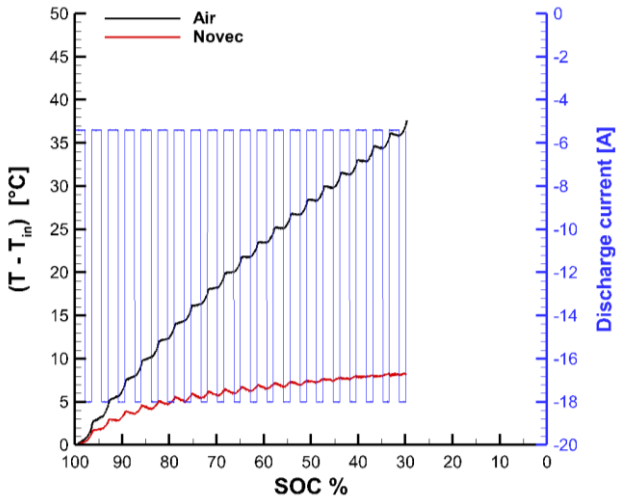

Figure 16. Battery temperature difference for the impulsive current test

7. CONCLUSIONS

In this study, an experimental investigation of direct immersion liquid cooling of a commercial $LiFePO_4$ Li-Ion battery is presented. The liquid used in this study is a dielectric fluid with a low boiling point. The cell under test was characterized from a thermal and electrical point of view: open circuit potential and EHC was experimentally measured, and a simplified equation was applied to determine the heat generation using battery surface temperature measurements. The thermal behavior of the cell submerged in the dielectric liquid was investigated under several operating currents. Both constant and impulsive current conditions were tested.

The results show that higher discharge currents lead to an increase in the thermal power because of the higher overpotential related to a greater battery voltage drop. The greatest thermal power generated was observed at low SOC because of the abrupt decay of voltage and the negative value of EHC. Consequently, also the temperature has a sharp increase and reaches very high values, especially at higher C-rates. The surface temperature of the battery at the end of discharge was strongly reduced when it was submerged in the dielectric liquid. This is particularly evident when the coolant is near the boiling point and the zones near the battery surface experience the change of phase. In this case, the thermal power generated is totally managed by the fluid, obtaining an almost constant temperature of the battery surface. This is due to the higher convective heat transfer coefficient associated to the nucleate boiling on battery surface and to the greater heat absorbed during the change of phase.

The obtained results show that the direct immersion cooling can manage the surface battery temperature even during severe operating conditions. The introduced strategy, based on a low boiling dielectric fluid, is really attractive because the change of phase allows to further reduce the surface temperature especially in case of instantaneous high electrical power requirements.

REFERENCES

[1] Masayoshi, W.A.D.A. (2009). Research and development of electric vehicles for clean transportation. Journal of Environmental Sciences, 21(6): 745-749. https://doi.org/10.1016/S1001-0742(08)62335-9

[2] De Wilde, H.P.J., Kroon, P. (2013). Policy options to reduce passenger cars CO_2 emissions after 2020. Energy Research Centre of the Netherlands, 5-35.

[3] Lowe, M., Tokuoka, S., Trigg, T., Gereffi, G. (2010). Lithium-ion batteries for electric vehicles. The US Value Chain, Contributing CGGC researcher: Ansam Abayechi.

[4] Karden, E., Ploumen, S., Fricke, B., Miller, T., Snyder, K. (2007). Energy storage devices for future hybrid electric vehicles. Journal of Power Sources, 168(1): 2-11. https://doi.org/10.1016/j.jpowsour.2006.10.090

[5] Speirs, J., Contestabile, M., Houari, Y., Gross, R. (2014). The future of lithium availability for electric vehicle batteries. Renewable and Sustainable Energy Reviews, 35: 183-193. https://doi.org/10.1016/j.rser.2014.04.018

[6] Matthe, R., Turner, L., Mettlach, H. (2011). VOLTEC battery system for electric vehicle with extended range. SAE International Journal of Engines, 4(1): 1944-1962.

[7] Li, X.W., Zhao, F., Hou, J.L., Guo, W. (2021). Features and spread mechanism of thermal runaway for electric car batteries. International Journal of Heat and Technology, 39(4): 1066-1074. https://doi.org/10.18280/ijht.390404

[8] Qin, P., Liao, M., Mei, W., Sun, J., Wang, Q. (2021). The experimental and numerical investigation on a hybrid battery thermal management system based on forced-air convection and internal finned structure. Applied Thermal Engineering, 195: 117212. https://doi.org/10.1016/j.applthermaleng.2021.117212

[9] Mohammadian, S.K., Zhang, Y. (2015). Thermal management optimization of an air-cooled Li-ion battery module using pin-fin heat sinks for hybrid electric vehicles. Journal of Power Sources, 273: 431-439. https://doi.org/10.1016/j.jpowsour.2014.09.110

[10] Wang, H., Tao, T., Xu, J., Mei, X., Liu, X., Gou, P. (2020). Cooling capacity of a novel modular liquid-cooled battery thermal management system for cylindrical lithium ion batteries. Applied Thermal Engineering, 178: 115591. https://doi.org/10.1016/j.applthermaleng.2020.115591

[11] Fang, Y., Ye, F., Zhu, Y., Li, K., Shen, J., Su, L. (2020). Experimental investigation on system performances and transient response of a pumped two-phase battery cooling system using R1233zd. Energy Reports, 6(s7): 238-247. https://doi.org/10.1016/j.egyr.2020.07.025

[12] Sirikasemsuk, S., Wiriyasart, S., Prurapark, R., Naphon, N., Naphon, P. (2021). Water/nanofluid pulsating flow in thermoelectric module for cooling electric vehicle battery systems. International Journal of Heat and Technology, 39(5): 1618-1626. https://doi.org/10.18280/ijht.390525

[13] Duan, X., Naterer, G.F. (2010). Heat transfer in phase change materials for thermal management of electric vehicle battery modules. International Journal of Heat

and Mass Transfer, 53(23-24): 5176-5182. https://doi.org/10.1016/j.ijheatmasstransfer.2010.07.044
[14] Li, Y., Du, Y., Xu, T., Wu, H., Zhou, X., Ling, Z., Zhang, Z. (2018). Optimization of thermal management system for Li-ion batteries using phase change material. Applied Thermal Engineering, 131: 766-778. https://doi.org/10.1016/j.applthermaleng.2017.12.055
[15] Putra, N., Sandi, A.F., Ariantara, B., Abdullah, N., Mahlia, T.M.I. (2020). Performance of beeswax phase change material (PCM) and heat pipe as passive battery cooling system for electric vehicles. Case Studies in Thermal Engineering, 21: 100655. https://doi.org/10.1016/j.csite.2020.100655
[16] Gan, Y., He, L., Liang, J., Tan, M., Xiong, T., Li, Y. (2020). A numerical study on the performance of a thermal management system for a battery pack with cylindrical cells based on heat pipes. Applied Thermal Engineering, 179, 115740. https://doi.org/10.1016/j.applthermaleng.2020.115740
[17] Chen, M., Li, J. (2020). Nanofluid-based pulsating heat pipe for thermal management of lithium-ion batteries for electric vehicles. Journal of Energy Storage, 32: 101715. https://doi.org/10.1016/j.est.2020.101715
[18] Song, Y.F., Liu, Z.G., Li, S.W., Jin, Q.Y. (2021). Design and optimization of an immersion liquid cooling system in internet datacenter. International Journal of Heat and Technology, 39(6): 1923-1929. https://doi.org/10.18280/ijht.390629
[19] Patil, M.S., Seo, J.H., Lee, M.Y. (2021). A novel dielectric fluid immersion cooling technology for Li-ion battery thermal management. Energy Conversion and Management, 229: 113715. https://doi.org/10.1016/j.enconman.2020.113715
[20] Wu, S., Lao, L., Wu, L., Liu, L., Lin, C., Zhang, Q. (2022). Effect analysis on integration efficiency and safety performance of a battery thermal management system based on direct contact liquid cooling. Applied Thermal Engineering, 201: 117788. https://doi.org/10.1016/j.applthermaleng.2021.117788
[21] Wu, N., Ye, X., Yao, J., Zhang, X., Zhou, X., Yu, B. (2021). Efficient thermal management of the large-format pouch lithium-ion cell via the boiling-cooling system operated with intermittent flow. International Journal of Heat and Mass Transfer, 170: 121018. https://doi.org/10.1016/j.ijheatmasstransfer.2021.121018
[22] Wang, Y.F., Wu, J.T. (2020). Thermal performance predictions for an HFE-7000 direct flow boiling cooled battery thermal management system for electric vehicles. Energy Conversion and Management, 207: 112569. https://doi.org/10.1016/j.enconman.2020.112569
[23] Bandhauer, T.M., Garimella, S., Fuller, T.F. (2011). A critical review of thermal issues in lithium-ion batteries. Journal of the Electrochemical Society, 158(3): R1. https://doi.org/10.1149/1.3515880
[24] Nieto, N., Díaz, L., Gastelurrutia, J., Alava, I., Blanco, F., Ramos, J.C., Rivas, A. (2012). Thermal modeling of large format lithium-ion cells. Journal of The Electrochemical Society, 160(2): A212. https://doi.org/10.1149/2.042302jes
[25] Manikandan, B., Yap, C., Balaya, P. (2017). Towards understanding heat generation characteristics of Li-Ion batteries by calorimetry, impedance, and potentiometry studies. Journal of The Electrochemical Society, 164(12): A2794. https://doi.org/10.1149/2.1811712jes
[26] Giammichele, L., D'Alessandro, V., Falone, M., Ricci, R. (2021). Thermal behaviour of a cylindrical Li-Ion battery. TECNICA ITALIANA-Italian Journal of Engineering Science, 65(2-4): 218-223. https://doi.org/10.18280/ti-ijes.652-412
[27] Giammichele, L., D'Alessandro, V., Falone, M., Ricci, R. (2022). Thermal behaviour assessment and electrical characterization of a cylindrical Lithium–ion battery using infrared thermography. Applied Thermal Engineering, 205: 117974. https://doi.org/10.1016/j.applthermaleng.2021.117974
[28] Rad, M.S., Danilov, D.L., Baghalha, M., Kazemeini, M., Notten, P.H.L. (2013). Adaptive thermal modeling of Li-ion batteries. Electrochimica Acta, 102: 183-195. https://doi.org/10.1016/j.electacta.2013.03.167
[29] Thomas, K.E., Bogatu, C., Newman, J. (2001). Measurement of the entropy of reaction as a function of state of charge in doped and undoped lithium manganese oxide. Journal of the Electrochemical Society, 148(6): A570. https://doi.org/10.1149/1.1369365
[30] Madani, S.S., Schaltz, E., Knudsen Kær, S. (2019). An experimental analysis of entropic coefficient of a lithium titanate oxide battery. Energies, 12(14): 2685. https://doi.org/10.3390/en12142685
[31] Bernardi, D., Pawlikowski, E., Newman, J. (1985). A general energy balance for battery systems. Journal of the Electrochemical Society, 132(1): 5. https://doi.org/10.1149/1.2113792

NOMENCLATURE

C	Nominal capacity, Ah
C_P	Specific heat capacity, $J \cdot kg^{-1} \cdot K^{-1}$
E_{acc}	Accumulated energy, J
E_d	Dispersed energy, J
EHC	Entropic heat coefficient, $mV \cdot K^{-1}$
I	Operating current, A
Pr	Prandtl number
Q	Thermal power, W
Q_{irr}	Irreversible thermal power, W
Q_{rev}	Reversible thermal power, W
SOC	State of charge
T	Temperature, K
t	Time, s
U_{OC}	Open circuit potential, V
V	Cell potential, V

Greek symbols

α	Thermal diffusivity, $m^2 \cdot s^{-1}$
λ	Thermal conductivity, $W \cdot m^{-1} \cdot K^{-1}$
ρ	Density, $kg \cdot m^{-3}$
τ	Discharge time, s

Subscripts

in	Initial value
e	Environment